Two Open States with Progressive Proton Selectivities in the Branched Channelrhodopsin-2 Photocycle

André Berndt,[△] Matthias Prigge,[△] Dietrich Gradmann,[*] and Peter Hegemann[*]
Institute for Biology, Experimental Biophysics, Humboldt-Universität zu Berlin, Berlin, Germany

ABSTRACT Channelrhodopsins are light-gated ion channels that mediate vision in phototactic green algae like *Chlamydomonas*. In neurosciences, channelrhodopsins are widely used to light-trigger action potentials in transfected cells. All known channelrhodopsins preferentially conduct H^+. Previous studies have indicated the existence of an early and a late conducting state within the channelrhodopsin photocycle. Here, we show that for channelrhodopsin-2 expressed in *Xenopus* oocytes and HEK cells, the two open states have different ion selectivities that cause changes in the channelrhodopsin-2 reversal voltage during a light pulse. An enzyme kinetic algorithm was applied to convert the reversal voltages in various ionic conditions to conductance ratios for H^+ and divalent cations (Ca^{2+} and/or Mg^{2+}), as compared to monovalent cations (Na^+ and/or K^+). Compared to monovalent cation conductance, the H^+ conductance, α, is ~3×10^6 and the divalent cation conductance, β, is ~0.01 in the early conducting state. In the stationary mixture of the early and late states, α is larger and β smaller, both by a factor of ~2. The results suggest that the ionic basis of light perception in *Chlamydomonas* is relatively nonspecific in the beginning of a light pulse but becomes more selective for protons during longer light exposures.

INTRODUCTION

Channelrhodopsins (ChRs) of *Chlamydomonas reinhardtii* are of wide interest because they are prototypes of light-gated channels that initiate vision in phototactic algae (1) and are widely used as neurophysiological tools to trigger action potentials by light in ChR2-transfected cells (2). In both respects, the selectivity of these channels is crucial. All known ChRs preferentially conduct H^+, but in physiological conditions and external pH_e between 6 and 8, Na^+, K^+, and Ca^{2+} can significantly contribute to the current (3–6). The relative preference of H^+ over Na^+ and K^+ has been estimated approximately ($>10^6$) from stationary currents at a fixed voltage and various ion concentrations (5,7).

Fig. 1 summarizes the known electrophysiological properties of ChR2. Typically, during a bright light stimulus of a few hundred milliseconds, the current decreases from an early peak to a stationary level (Fig. 1 *A*) (7,8). This feature, and the finding that the peak is smaller upon a second light pulse after a brief dark period (7,9), led to the proposal of a branched photocycle with two conducting (open) states, O_1 and O_2, and two nonconducting (closed) states, C_1 and C_2 (Fig. 1 *B*) (9,10). Because the transition from C_2 to C_1 is irreversible, the model in Fig. 1 *B* dictates that in the first instant of illumination after a long dark period, only O_1 will be occupied before O_2 is populated from O_1 and C_2. Thus, the initial current, I_0, obtained by extrapolation of the current relaxation from peak to stationary level to time zero (see Fig. 1 *A*), can be assigned solely to the early state O_1, whereas the peak itself already comprises some conversion of O_1 to O_2, because the peak marks the time when the decrease of the current through O_1 and the increase of the current through O_2 cancel each other to yield zero temporal slope of the total current. At low-intensity light pulses, the peak current appears later due to successive ChR activation and is smaller due to low occupancy of the O2 state. In fact, when our analysis below was carried out using the peak currents instead of the initial currents (results not shown), the qualitative features were similar but not as strongly expressed as from the actual analysis presented here. Compared to I_0, the stationary current, I_∞, reflects a mixture of currents through O_1 and O_2 but with more contribution from O_2. For a given voltage, the model allows identification of time courses of occupancy for all four states, and conductivity for the two open states (9,10), but does not allow conclusions to be drawn with respect to their ionic selectivity. Strictly speaking, C_1 and C_2 represent the ensemble of several nonconducting states that were previously identified by spectroscopy (3,11,12).

The aim of this study is a systematic investigation of the selectivities of the two ChR2 conducting states. Previous reports of other ion channels with states of different ion selectivity were merely qualitative and based on current amplitudes at a fixed holding voltage (13). In contrast, Lin et al. considered reversal voltages for ChR2, but did not discriminate between early and late currents (6). This study is based on reversal voltages and a quantitative selectivity analysis based on the enzyme kinetic reaction scheme in Fig. 1 *C*. The benefit of this model is that the reversal voltage is expressed by only one substrate parameter per ion species. In contrast, the more familiar model of a substrate binding site between two barriers requires three independent parameters per ion species.

Submitted May 6, 2009, and accepted for publication October 19, 2009.

[△] André Berndt and Matthias Prigge contributed equally to this work.

*Correspondence: dgradma@gwdg.de or hegemape@rz.hu-berlin.de

Dietrich Gradmann's present address is A.-v.-Haller-Institut der Universität, 37073 Göttingen, Germany.

Editor: Michael Pusch.

0006-3495/10/03/0753/9 $2.00

doi: 10.1016/j.bpj.2009.10.052

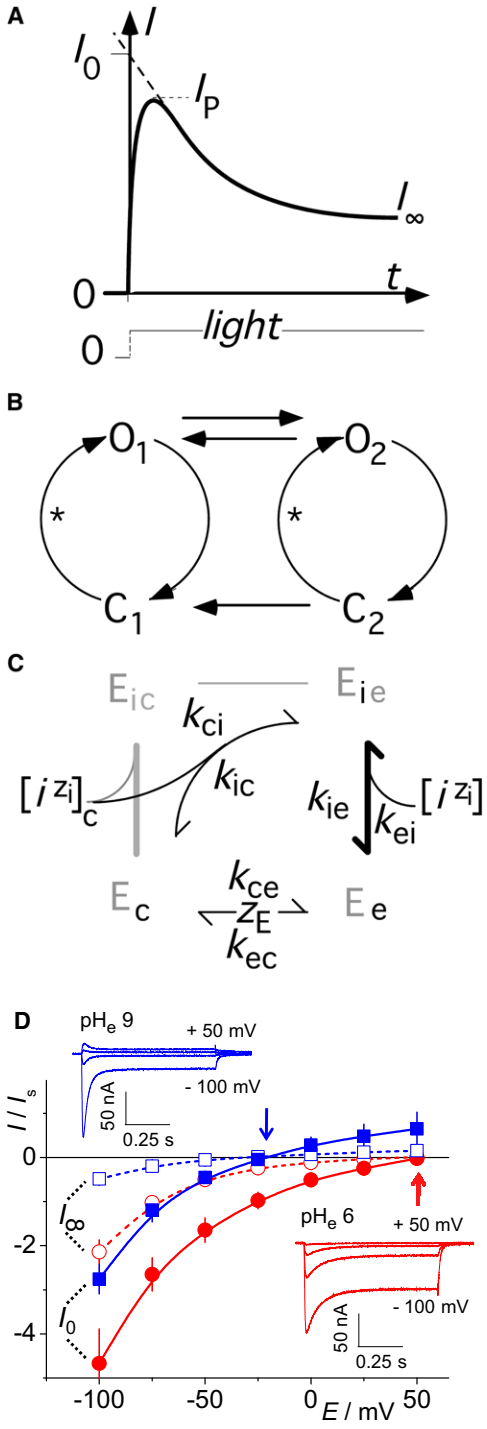

FIGURE 1 Definitions, recapitulation, and reaction schemes of the working hypothesis. (*A*) Typical time course of ChR2 photocurrent upon a bright, rectangular light pulse: after an early peak (I_P), the current relaxes to a stationary level, I_∞; extrapolation of the steepest slope to $t = 0$ yields the initial current, I_0. (*B*) Simplified photocycle of ChR (6,7) with early and late conducting (open) states O_1 and O_2, respectively, plus two nonconducting (closed) states, C_1 and C_2. Asterisks indicate photoisomerization steps. Due to the irreversible step from C_2 to C_1, the steady-state occupation probabilities, p, of the four states are $p_{C1} = 1$, and $p_{O1} = p_{O2} = p_{C2} = 0$ in the dark; hence, I_0 can be assigned to state O_1 exclusively. (*C*) Reaction scheme for experiments with concentration changes of external ions; bold line indicates rapid equilibria. Derivation of three-state model from standard four-state model (*gray*) for uniport of one substrate *i* through enzyme E when no internal concentration changes take place. Subscripts c and e represent cytoplasmic and external measures, respectively. In the global model, *n* ion species, *i*, with their specific valencies, z_i, compete for the empty binding site with charge z_E, resulting in *n* three-state cycles sharing reorientation of the empty binding site between the cytoplasmic and external sides. (*D*) Current-voltage relationships for current amplitudes of I_0 and I_∞ versus holding voltage, recorded at pH_e 9 and 6. I_S is the reference current at pH_e 7.5 with 100 mM external Na^+, for standardizing results from various preparations. Arrows indicate the estimated reversal voltages, and insets show individual current tracings at the indicated holding voltages.

Fig. 1 *D* illustrates previous observations regarding ChR photocurrents as they occur upon stimulation with bright light pulses (7,8), showing the sensitivity of the initial current (I_0) and the stationary currents (I_∞) to external pH, pH_e, and transmembrane voltage, *E*, over wide ranges: The ratio I_0/I_∞ is quite variable but always >1 in response to pulses of bright light. This ratio decreases with acidic pH_e and positive voltages. These striking features of the current amplitudes are of minor interest in this study, as they do not help the observer to draw conclusions about the relative selectivities of O_1 and O_2. Thus, we focus on conditions where the currents reverse their sign at the reversal voltages, E_r.

The positive shift of the reversal voltages upon external acidification (Fig. 1 *D*, *arrows*) identifies H^+ as the prevalent charge carrier of the ChR2 photocurrents. Differences between reversal voltages E_{r0}, determined from initial currents, and $E_{r\infty}$ from stationary currents, are barely discernable from plots such as those in Fig.1 *D*. However, such differences could exist and indicate different ion selectivities of those two states. These differences could, in fact, be assessed by more detailed investigations of photocurrents near the reversal voltage in various ionic conditions.

Since different ion species will not move independently through ChR2 and since Ca^{2+}can also pass ChR2 (5–7), it is, to our understanding, illegitimate to convert the reversal voltages to conductance ratios by the familiar formalism of the Goldman equation, although this has been done by Lin and colleagues (6) using a modified GHK algorithm according to Chang (14). We used instead an alternate, enzyme kinetic algorithm, which is presented in detail below. The use of an enzyme kinetic model with a defined binding site instead of a single barrier is necessary, because all transportable ion species will compete for passage through the selectivity filter and impede the passage of alternate ions by temporal occupation of the binding site(s).

One simple model to account for competition would be one binding site between two barriers. A quantitative treatment of the selectivity problem with this model would require three independent parameters for each translocated species (not illustrated), i.e., nine free parameters for the three different ion species investigated here. As an alternative, our applied model (Fig. 1 *C*) with fast binding equilibria

and slow reorientation steps requires only one species-specific parameter for a quantitative treatment of the selectivity problem (see Theoretical, in Materials and Methods).

MATERIAL AND METHODS

Experimental

Voltage-clamp experiments on heterologously expressed ChR2 were carried out in *Xenopus* oocytes and HEK293 cells (here, HEK cells), as described previously (4,7).

Experiments in *Xenopus* oocytes were carried out under various ionic conditions (in mM): 0.1 $CaCl_2$, 2 $MgCl_2$, and 100 NMGCl or 100 NaCl at pH 9 (5 glycine), pH 7.5 (5 MOPS), or pH 6 (5 MES). For an increase of Ca^{2+}, 1 mM NMG was replaced by 1 mM $CaCl_2$. Detailed voltage-clamp recordings of initial and stationary currents were carried out at holding voltages, E_C, in the vicinity of reversal voltages; E_r was determined as the intersection of the regression line with zero current line.

An HEK293 cell line expressing ChR2-WT(1–307) inducible by adding 1 μM tetracycline was the kind gift of E. Bamberg (MPI Frankfurt, Frankfurt, Germany). Cells were cultured in Dulbecco's minimal essential medium supplemented with 10% (v/v) fetal bovine serum, 2 mM glutamine (Biochrome, Berlin, Germany), 175 μM penicillin, 68 μM streptomycin, 120 μM blasticidine, and 175 μM zeocine. Cells were seeded on coverslips at a concentration of 0.4×10^6 cells/ml. One day after seeding, cells were induced by 1 μM tetracycline. At 20 h postinduction, currents in cells were recorded with a conventional whole-cell patch-clamp method with an Axopatch200B and a Digidata 1440 (Molecular Devices, Sunnyvale, CA). The external solution contained (in mM) 100 NaCl, 2 $CaCl_2$, and 2 $MgCl_2$ with 10 HEPES (pH_e 7.5), 10 Tris (pH_e 9.0), or 10 MES (pH 6.0). The internal cytoplasmic solution contained (in mM) 120 NaCl, 10 EGTA, 2 $MgCl_2$, 2 $CaCl_2$, and 10 HEPES (pH_c was adjusted to 7.3 using either CsOH or HCl). In all experiments, salt bridges were used to keep the electrodes at 100 mM NaCl under all conditions.

A 75-W xenon lamp (Jena Instruments, Jena, Germany) combined with a fast shutter (Uniblitz T132; Vincent Associates, Rochester, NY) was used for light pulses. Blue light was selected with a dichroic mirror reflecting 450–490 nm light through the objective onto the sample. 100% light intensity corresponded to 4.5×10^{21} photons m^{-2} s^{-1} at the cell surface.

Theoretical

The formalism of the Goldman equation applies not only to independent electrodiffusion but also to cases where several ion species compete for the main binding site of a charge-translocating enzyme (15). However, this holds only if the competing ion species have the same valency. Here, we develop an algorithm that makes it possible to determine selectivity relations from reversal voltages as well as for enzymatic translocation of ions with different valencies.

Formalism

Let us assume a standard four-state transport cycle (Fig. 1 *C*) with fast binding equilibria and slow reorientation steps. If the internal medium is not changed during experimentation, only the parameters of a three-state model can be identified from steady-state current-voltage relationships, whereby the inner equilibrium and the reorientation of the loaded state is lumped as a pair of gross rate constants (16).

Fig. 1 *C* illustrates this scenario for n ion species i with valencies z_i. When z_i is different for the different species, the reversal voltage depends on the fundamental rate constants k^0_{ce} and k^0_{ci}, and on the ion concentrations on both sides in the following manner. Reorientation of the empty binding site is defined as

$$k_{ce} = k^0_{ce}\exp(+z_E u/2) \tag{1a}$$

$$k_{ec} = k^0_{ec}\exp(-z_E u/2), \tag{1b}$$

where subscripts "c" and "e" stand for cytoplasmic and external, respectively, and superscript "0" identifies reference conditions (0 mV, 1 mM). The reduced membrane voltage, u, is defined as $u = EF/(RT)$. Rate constants are expressed in s^{-1}.

Gross rate constants for binding/unbinding and reorientation of the occupied binding site are written

$$k_{ci} = k^0_{ci}\exp(+(z_E + z_i)u/2)[i]_c \tag{1c}$$

$$k_{ic} = k^0_{ic}\exp(-(z_E + z_i)u/2). \tag{1d}$$

Rapid, external binding equilibria are $K_i = k_{ei}/k_{ie}$ at k_{ei}, $k_{ie} >> k_{ci}$, k_{ic}, k_{ec}, k_{ce} with

$$K_i = K^0_i[i]_e \tag{2a}$$

$$K^0_i = k^0_{ec}k^0_{ci}/\left(k^0_{ic}k^0_{ce}\right), \tag{2b}$$

because of microscopic reversibility.

We use auxiliary weighting variables, F, for King-Altman determination of state probabilities (17). Derivation and application of these weighting variables is demonstrated by the following example: with two assumed substrates, 1 and 2, Fig. 1 *C* becomes a four-state model, i.e., two three-state cycles sharing the empty site with its two orientation states c and e, plus the two loaded states E_1 and E_2 ($n = 2$) . For each of the four states, there are eight product combinations of three rate constants, which feed the population of the respective state at the expense of the other three states; and the sum of these combinations amounts to the respective weighting factor, F. For state c, these combinations are $k_{ec}k_{1c}k_{2c}$, $k_{ec}k_{1c}k_{2e}$, $k_{ec}k_{2c}k_{1e}$, $k_{ec}k_{1e}k_{2e}$, $k_{1e}k_{e2}k_{2c}$, $k_{2e}k_{e1}k_{1c}$, $k_{1c}k_{2c}k_{e1}$, and $k_{1c}k_{2c}k_{e2}$; corresponding combinations hold for the other states. Because of condition 2, k_{e1}, k_{1e}, k_{e2}, $k_{2e} >> k_{c1}$, k_{1c}, k_{2c}, $k_{c2,}$ k_{ce}, k_{ec}, five of these eight combinations can be ignored, leaving three relevant combinations, namely $k_{ec}k_{1c}k_{2e}$, $k_{1e}k_{e2}k_{2c}$, and $k_{2e}k_{e1}k_{1c}$, for state c, with corresponding combinations for the other states. Dividing all terms by the products of the fast reactions $k_{1e}k_{2e}$ and substituting $K_1 = k_{e1}/k_{1e}$ and $K_2 = k_{e2}/k_{2e}$ yields the sum $F_c = k_{ec} + k_{1c}K_1 + k_{2c}K_2$ as a weighting variable for state c, with corresponding sums for the other three states. Application of these rules for n substrates i yields

$$F_c = k_{ec} + \sum k_{ic}K_i \tag{3a}$$

$$F_e = k_{ce} + \sum k_{ci} \tag{3b}$$

$$F_i = K_i F_e. \tag{3c}$$

To normalize the system to a total occupation probability of 1, we form the denominator

$$\mathrm{Den} = F_c + F_e + \sum F_i, \tag{4}$$

which allows us to calculate the individual state probabilities as

$$p_c = F_c/\mathrm{Den} \tag{5a}$$

$$p_e = F_e/\mathrm{Den} \tag{5b}$$

$$p_i = F_i/\mathrm{Den} \tag{5c}$$

The currents through the individual limbs are

$$I_E = e \times z_E(p_c k_{ce} - p_e k_{ec}) \tag{6}$$

for the empty binding site, where e is the elementary charge and z_E the charge number of the empty binding site, and

$$I_i = e \times (z_E + z_i)(p_c k_{ce} - p_i k_{ic}) \tag{6i}$$

for the loaded sites. So the total current is

$$I = I_E + \sum I_i. \tag{7}$$

This sum does not reflect independence among the various ion species; instead, Eq. 6i indicates the interaction, as all rate constants of the system enter the occupation probability, p, of each state (Eq. 5) via Eqs. 3, a–c, and 4.

The following relationships prove that the reversal voltage, $E_r = E_{I=0}$, is independent of k_{ec}, k_{ic}, and z_E. For zero current, $I_E + \Sigma I_i = 0$, we use Eq. 6. to write

$$e \times z_E(p_c k_{ce} - p_e k_{ec}) + \sum \{e \times (z_E + z_i)(p_c k_{ce} - p_i k_{ic})\} = 0. \tag{8a}$$

Dividing both terms by e and Den yields the net fluxes through the $n + 1$ pathways

$$z_E(F_c k_{ce} - F_e k_{ec}) + \sum \{(z_E + z_i)(F_c k_{ci} - F_i k_{ic})\} = 0, \tag{8b}$$

or the net charge fluxes, rightward minus leftward,

$$\begin{aligned} &F_c\left\{z_E k_{ce} + \sum((z_E + z_i)k_{ci})\right\} \\ &- F_e\left\{z_E k_{ec} + \sum((z_E + z_i)K_i k_{ic})\right\} = 0, \end{aligned} \tag{8c}$$

which, when F is substituted by Eq. 3, becomes

$$\begin{aligned} &\left\{k_{ec} + \sum(k_{ic}K_i)\right\}\left\{z_E k_{ce} + \sum((z_E + z_i)k_{ci})\right\} \\ &- \left\{k_{ce} + \sum k_{ci}\right\}\left\{z_E k_{ec} + \sum((z_E + z_i)K_i k_{ic})\right\} = 0. \end{aligned} \tag{8d}$$

Introducing the voltage and concentration dependences of Eqs. 1 and 2. and using the symbols $e_0 = \exp(z_E u/2)$, $e_i = \exp(z_i u/2)$, and $e_I = \exp((z_E + z_i)u/2)$ for momentaneous writing economy, yields

$$\begin{aligned} &\left\{k^0_{ec}/e_0 + \sum\left(k^0_{ic}/e_I \frac{k^0_{ec}k^0_{ci}}{k^0_{ce}k^0_{ic}}[i]_e\right)\right\}\left\{z_E k^0_{ce} e_0 + \sum\left((z_E + z_i)k^0_{ci} e_I [i]_c\right)\right\} = \\ &\left\{k^0_{ce}/e_0 + \sum\left(k^0_{ci}[i]_c e_I\right)\right\}\left\{z_E k^0_{ec}/e_0 + \sum\left((z_E + z_i)\frac{k^0_{ec}k^0_{ci}}{k^0_{ce}k^0_{ic}}[i]_e k^0_{ic}/e_I\right)\right\}. \end{aligned} \tag{9}$$

Multiplication of both sides (left side first, then right side) by k^0_{ce}/k^0_{ec}, shortening by k^0_{ic} and e_0, and subtraction of the z_E expressions from both sides yields

$$\begin{aligned} &\left\{k^0_{ce} + \sum\left(k^0_{ci}[i]_e \exp(-z_i u/2)\right)\right\}\left\{k^0_{ce} + \sum\left(z_i k^0_{ci}[i]_c \exp(z_i u/2)\right\}\right. = \\ &\left\{k^0_{ce} + \sum(k^0_{ci}[i]_c \exp(z_i u/2))\right\}\left\{k^0_{ce} + \sum(z_i k^0_{ci}[i]_e \exp(-z_i u/2)\right\}. \end{aligned} \tag{10}$$

In this form, z_E and the fundamental rate constants k^0_{ec} and k^0_{ic} do not appear any more. Q.E.D.

For z_i = constant, k^0_{ce} drops out as well, and Eq. 10 assumes the form of the Goldman equation after some rearrangement:

$$\frac{\sum\left(k^0_{ci}[i]_c\right)}{\sum\left(k^0_{ci}[i]_e\right)} = \exp(-z_i u), \tag{11}$$

confirming Eq. 97 in Andersen (15).

RESULTS AND DISCUSSION

Qualitative observations

ChR2 was expressed in *Xenopus* oocytes and photocurrents were recorded under various ionic and voltage conditions in response to bright light pulses of 450 nm. To examine a possible anion conductance, the 100-mM external Cl^- was partially or totally replaced by alternate anions, like glutamate, aspartate, or sulfate, which were assumed to have an even smaller conductance in ChR2 than Cl^-. All three ions reduced the current amplitudes up to 25% at concentrations between 0 and 5 mM. However, none of the ions caused E_r to become more positive. Similar experiments were repeated in ChR2-expressing HEK cell lines. Again, partial exchange of cytoplasmic Cl^- by aspartate did not affect E_r, so a significant anion conductance of ChR2, especially for Cl^-, was excluded.

In contrast, partial or total replacement of inorganic cations in oocytes and HEK cells in the bath by the large organic NMG^+, caused E_r to become more negative throughout, confirming the observations from studies cited above. Since K^+ and Na^+ had similar effects (5–7), for quantitative purposes, we subsumed these ions under M^+, meaning the sum of the monovalent ions K^+ and Na^+.

Likewise, a major increase of external Ca^{2+} or Mg^{2+} from 2 to 20 mM, caused noticable depolarization, especially at pH_e 9 in the absence of external M^+. Since the conductances of Ca^{2+} and Mg^{2+} could not be distinguished in a first series of experiments, we subsumed these divalent cations under

D^{2+} for quantitative considerations. For maintaining the stability of the preparations, external D^{2+} could not totally be replaced.

Quantitative aspects

To determine the reversal voltages precisely, we recorded the current-voltage relationship of ChR2 in the vicinity of the reversal voltages with small voltage intervals. Typical results of this approach are shown in Fig. 2 for ChR2 in *Xenopus* oocytes. In the absence of external Na^+ (Fig. 2 *A*), the initial reversal voltage and the stationary reversal voltage can hardly be distinguished at any pH_e. However, in the presence of 100 mM external Na^+, the differences are obvious. The stationary reversal voltages are more negative than those for the initial current and this difference is most pronounced at pH_e 9. The more negative reversal voltage indicates an increased H^+ selectivity in the stationary state compared to the initial one, because the Nernst equilibrium voltage for H^+, $E_H = RT/F \times \ln([H^+]_e/[H^+]_c)$ was near −100 mV at pH_e 9, whereas E_M and E_D were close to zero.

Consequently, the time courses of the photocurrents at clamp voltages near the reversal voltage are of particular interest (Fig. 2 *C*). Data for pH_e 9 in Fig. 2 *B* indicate that for certain holding voltages between the initial and the

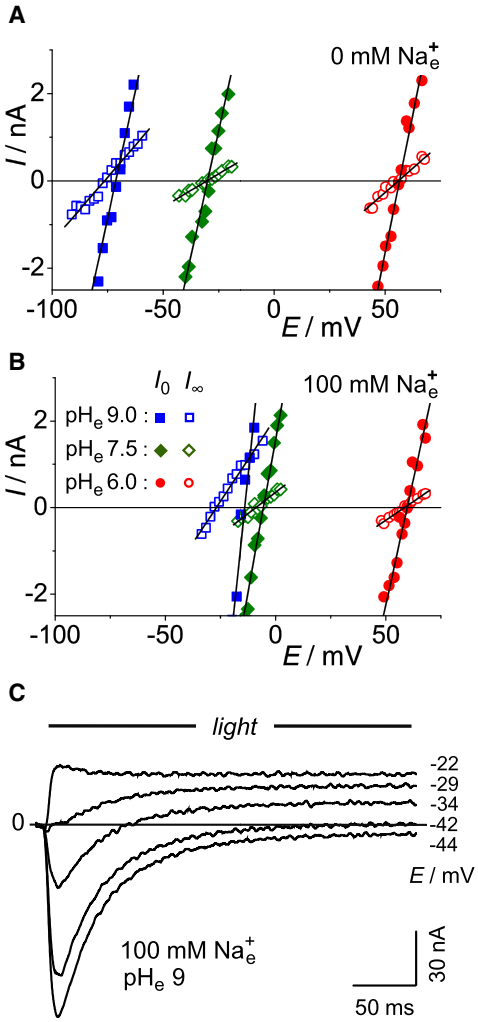

FIGURE 2 Typical experiment for determination of reversal voltages E_{r0} and $E_{r\infty}$ of ChR2 in *Xenopus* oocytes under various ionic conditions (in mM): internal, ~120 Na^+, ~40 Cl^-, pH_c 7.3; external, 0.1 $CaCl_2$, 2 $MgCl_2$, and 100 mM NMGCl (*A*) or 100 mM NaCl (*B*). Voltage-clamp recordings of initial and stationary currents, *I*, were carried out at holding voltages, E_C, in the vicinity of reversal voltages. Readings of E_r are from intersections of regression lines with the zero-current line in the absence of external Na^+ (A), and in the presence of 100 mM external Na^+ (*B*) (for statistical evidence, see Fig. 4 *D*; for quantitative analysis, see Table 1). (*C*) Original photocurrent records, measured at the indicated holding voltages. Note change of current sign in middle tracing (−34 mV), indicating change of reversal voltage and selectivity during a light pulse. Since the experiments in *A–C* were from different oocytes, the current scale in *C* was adjusted to match *A* and *B*.

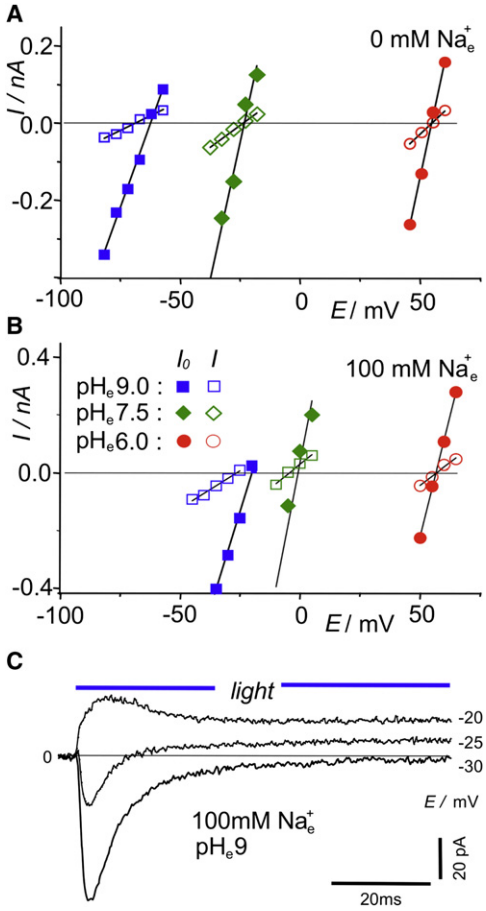

FIGURE 3 Typical experiment for determination of reversal voltages E_{r0} and $E_{r\infty}$ of ChR2 in HEK cells under various ionic conditions (in mM): internal, 120 NaCl, 10 Hepes, 2 $MgCl_2$, 10 EGTA, and 2 $CaCl_2$, pH_c 7.3; and external, 2 $CaCl_2$, 2 $MgCl_2$, and 100 mM NMGCl (*A*) or 100 mM NaCl (*B*). Voltage-clamp records of initial and stationary currents, *I*, are shown at holding voltages, E_C, in the vicinity of reversal voltages. Readings of E_r are from intersections of regression lines with the zero-current line. in the absence of external Na^+ (*A*), and with 100 mM added external Na^+ (*B*). The predominant result was $E_{r\infty} < E_{r0}$ throughout, indicating increased H^+ selectivity in the stationary state compared to the initial state (for statistical evidence, see Fig. 4 *A*, and for quantitative analysis, see Table 1). (*C*) Original photocurrent records. Note change of current sign in the middle tracing (−25 mV), indicating change of reversal voltage and selectivity during a light pulse. The current scale was adjusted to match *A* and *B*.

stationary reversal voltage, the initial current will be negative and the stationary current positive, with a change of sign in between. This scenario is well represented by the current tracing at a holding voltage of −34 mV in Fig. 2 *C*.

Another interesting case is the current record for −42 mV in Fig. 2 *C*, where the holding voltage equals the stationary reversal voltage, yielding zero stationary current: whereas the initial currents are assigned to the early state O_1 exclusively, according to the model of Fig. 1 *B*, the stationary current is a mixture of currents through both states, O_1 and O_2. Consequently, zero total stationary current implies equal amounts of 1), M^+- and D^{2+}-dominated inward current through O_1, and 2), H^+-dominated outward current through O_2.

Electrophysiological studies in *Xenopus* oocytes bear some uncertainty, because the actual ionic composition of cytoplasmic medium is not known exactly but has to be assumed from the literature (18). To avoid this disadvantage, similar experiments were performed with HEK cells as well, where the experimenter sets the ionic composition of the internal medium. The results of such a typical experiment are shown in Fig. 3. Here, the reversal voltages, especially those in the alkaline pH_e range, are more positive than those from *Xenopus* ooytes (see Eq. 1).

The main conclusions of this study are based on the differences between the initial and the stationary reversal voltages, E_{r0} and $E_{r\infty}$. The differences in HEK cells are smaller than for ChR2 in oocytes, and the significance of these differences is not evident in Fig. 4, *A* and *B*. Therefore, these differences are plotted with statistical support by Fig. 4, *C* and *D*, for the ionic condition pH_e 9. These panels show significantly more negative $E_{r\infty}$ than E_{r0} in the presence of 100 mM Na^+_e. This shift toward the dashed reference line (E_H) in Fig. 4, *A* and *B*, indicates an increased H^+ selectivity.

Before the observed changes of the reversal voltages are quantitatively analyzed in terms of selectivity, alternative explanations should be considered. In particular, it is conceivable that the concentration terms in Eq. 10 change during continuous current clamping because of formation of unstirred depletion and accumulation layers in the close vicinity of membranes. Fortunately, a major bias by this mechanism can be excluded, because measurements of E_r in flowing or stagnant media resulted in E_r changes of only a few percentage points both in *Xenopus* oocytes and in HEK-cells, rendering these effects irrelevant in our context.

The mean experimental data of the pH_e- and $[M^+]_e$-dependent reversal voltages of ChR2 in HEK cells are plotted versus pH_e in Fig. 4 *A*. The dashed auxiliary line with the reference slope $m = 1$ of 59 mV/pH unit, marks the Nernst equilibrium voltage for protons, $E_H = RT/F \times \ln([H^+]_e/[H^+]_c)$, at different pH_e values. This reference line crosses the $E_r = 0$ line when $pH_e = pH_c$.

The data points at pH_e 9 in the absence of external M^+ are more positive than E_H marked by the dotted reference line. Since at $[M^+]_e = 0$, E_M is more negative than E_H, the observed deviation must be due to an $E_X > E_H$, where X might be Cl^- ($E_{Cl} \approx 0$ mV), Ca^{2+} ($E_{Ca} \approx +120$ mV), or Mg^{2+} ($E_{Mg} \approx 0$ mV) in these conditions. Since a significant role of anions has already been excluded, and since the impact of Mg^{2+} and Ca^{2+} is similar (see qualitative observations above), we assign this difference to the global selectivity of divalent ions, D^{2+} (Mg^{2+} and Ca^{2+}), compared to monovalent ions, M^+ (K^+ and Na^+), by the selectivity coefficient $\beta = k^0_{cD}/k^0_{cM}$ for divalent cations, in analogy with the selectivity coefficient $\alpha = k^0_{cH}/k^0_{cM}$, for H^+.

In principle, the coefficient γ (k^0_{ce}/k^0_{cM}) for the empty binding site is equivalent in interest to α (k^0_{cH}/k^0_{cM}) and

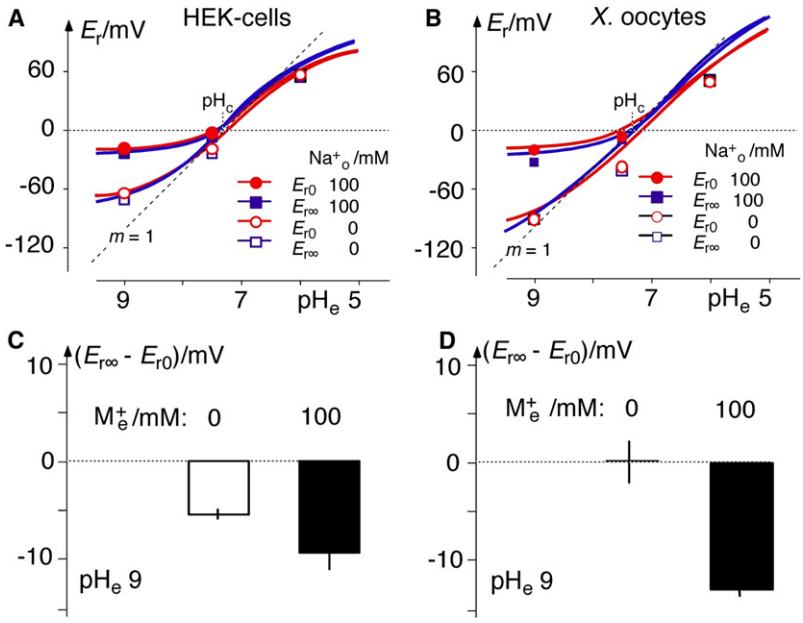

FIGURE 4 Initial (*red*) and stationary (*blue*) reversal voltages, E_{r0} and $E_{r\infty}$, of ChR2 as a function of pH_e, recorded with and without 100 mM external Na^+ in HEK cells and *Xenopus* oocytes. Values are means of $n \geq 3$ independent recordings. (*A*) Absolute E_r values in HEK cells (internal ion concentrations, in mM: 120 NaCl, 10 Hepes, 2 $MgCl_2$, 2 $CaCl_2$, and 10 EGTA, pH_c 7.3); small SEs of 0.5–5.7 mV ($n = 3$) not illustrated. dotted line: theoretical Nernstian $E_H(pH_e)$ with slope $m = 1$ (here, rounded 60 mV/pH unit); solid lines: theoretical relationships according to Eq. 10 with mean conductance ratios α and β from Table 1 at pH_c 9.0, with and without 100 mM Na^+_e. (*B*) Same as *A*, but for *Xenopus* oocytes (internal ion concentrations, in mM: 120 Na^+, 40 Cl^-, pH_c 7.4; data taken from Zhang and Prigge (4); small SEs of 1.0–5.0 mV (n = 3–7) are not shown. (*C* and *D*) Statistically supported differences, $E_{r\infty} - E_{r0}$, at pH_e 9, for HEK cells and *Xenopus* oocytes, respectively.

β (k^0_{cD}/k^0_{cM}). Fig. 5 *A* shows the theoretical impact of increasing and decreasing coefficients α, β, and γ, on the E_r(pCa) relationship of ChR2, where the reference curve with rounded parameters (Fig. 5 *A*, *inset*) basically reflects the experimental results. These changes need not be discussed here in full detail. However one feature worth noting in our specific scenario is that increases of γ can hardly be distinguished from decreases of β. Therefore, $\gamma = 1$ was fixed for numerical analysis by Eq. 10.

It is of interest that the E_r values in Fig. 4, *A* and *B*, show a correspondingly negative deviation from E_H at acidic pH_e. This observation reflects the scenario of Fig. 1 *C* and Eq. 10, when ions with different valencies compete with each other for translocation, whereas the familiar formalism of the Goldman equation would show an asymptotic approach of E_r to E_H for large and increasing $[H^+]_e$.

The simple observation that the $E_{r\infty}$ values from the stationary currents (Fig. 4, *blue line*) are closer to the dotted reference line, E_H, than are the E_{r0} values from the initial currents (*red*) already indicates a higher H^+ selectivity of ChR2 after longer illumination. The close coincidence of the fitted curves with the experimental data in Fig. 4 *A* confirms the validity of the analysis. It is pointed out that the numerical analysis was based only on the data at pH_e 9 and revealed good predictions for the measurements at pH_e 7.5 and pH_e 6.

To determine whether the results from experiments in HEK cells are representative for ChR2 or are biased by the particular expression system, analysis corresponding to that in Fig. 4 *A* has been carried out with ChR2 expressed in *Xenopus* oocytes. These results are plotted in Fig. 4 *B* and show basic agreement with those in Fig. 4 *A*, although in the absence of external Na^+, the deviation of the reversal voltages from the E_H is significantly smaller in *Xenopus* oocytes (Fig. 1 *B*) than in HEK cells (Fig. 4 *A*). This deviation is explained by the different concentrations of external Ca^{2+} in the two preparations: 2 mM Ca^{2+} in the HEK cell experiments, and 0.2 mM in the oocyte experiments. Taking this into account, similar conductance ratios were calculated for ChR2 in both expression systems (Table 1). The fact that the fits and predictions in Fig. 4 *B* are not as good as those in Fig. 4 *A* is explained by the uncertainties of the actual ionic composition of the cytoplasm in *Xenopus* oocytes, whereas in HEK cells, this composition was fully controlled by the experimenter.

The experimental results described in Fig. 4 directly demonstrate the behavior of the H^+ and M^+ conductances, whereas the role of D^{2+}, which was not changed during the experimentation, was only an indirect result of the analysis. This deficit was accounted for by direct demonstration

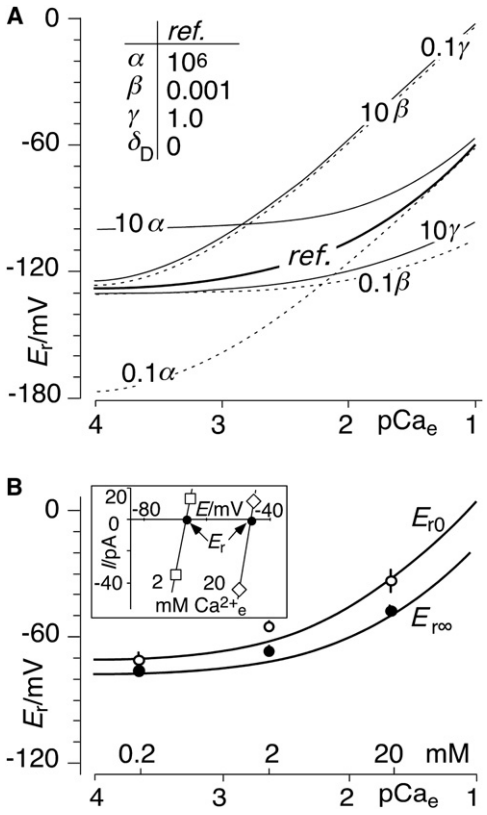

FIGURE 5 Effect of divalent cations, D^{2+} (Mg^{2+} + Ca^{2+}), on E_r. (*A*) Theoretical relations: impact of 10-fold increase and decrease of conductance ratios α (k^0_{cH}/k^0_{cM}), β (k^0_{cD}/k^0_{cM}), and γ (k^0_{ce}/k^0_{cM}) on $E_r([D^{2+}]_e)$ relationships compared to reference configuration (*inset*). Note that increase of γ and decrease of β are almost equivalent in this configuration ($[M^+]_c$ = 120 mM (100 mM K^+ and 20 mM Na^{2+}), $[D^{2+}]_c$ = 2 mM (2 mM Mg^{2+} and 0.25 μM Ca^{2+}), pH_c 7.3, pH_e $[M^+]_e = 0$, $[D^{2+}]_c$ as marked by pCa_e on abscissa). To circumvent corresponding fluctuations in fits, γ was arbitrarily fixed at $\gamma = 1$ for numerical analysis. (*B*) Experimental results (*symbols*, means ± SE) and fits (*solid lines*) of E_r at various external $[Ca^{2+}]$; cytoplasmic ions, $\gamma = 1$, $[M^+]_e = 0$, pH_e 9.0, as in *A*. To obtain fair fits, an ad hoc correction, δ_D, was introduced to account for the impact of external Mg^{2+}: $[D^{2+}]_e = \delta_D + [Ca^{2+}]_e$ (see numerical results in Table 2). (*Inset*) Example of original current-voltage data for ChR2 in HEK cells (pH_e 9, $[M^+]_e = 0$, internal solution, as in main figure) showing $[Ca^{2+}]_e$ dependency of E_r.

TABLE 1 ChR2 conductance ratios α, β, and γ in HEK cells and *Xenopus* oocytes

	HEK cells	*Xenopus* oocytes
α_0	4.5×10^6 ± 15%	3.0×10^6 ± 8%
α_∞	6.5×10^6 ± 16%	8.6×10^6 ± 13%
α_0/α_∞	0.71 ± 2%	0.36 ± 6%
β_0	18×10^{-3} ± 28%	5.5×10^{-3} ± 29%
β_∞	12×10^{-3} ± 31%	2.7×10^{-3} ± 37%
β_0/β_∞	1.56 ± 6%	2.2 ± 6%

$\alpha = k^0_{cH}/k^0_{cM}$ for H^+ over M^+ (Na^+ + K^+); $\beta = k^0_{cD}/k^0_{cM}$ for D^{2+} (Ca^{2+} + Mg^{2+}) Ca^{2+} over M^+; and $\gamma = k^0_{ce}/k^0_{cM} = 1$ in *Xenopus* oocytes and HEK-cells, determined by fitting Eq. 10 to pairs of reversal voltages, E_r, at pH_e 9.0 with and without 100 mM external Na^+, using experimental data presented in Fig. 4, *A* and *C*. Cytoplasmic cation concentrations were 120 mM M^+ (100 mM K^+ + 20 mM Na^+) and 2 mM D^{2+} (2 mM Mg^{2+} + 0.25 μM Ca^{2+}), pH_c 7.3. Subscripts 0 and ∞ indicate values from initial and stationary currents, respectively. Values are expressed as means ± percent error, 100·SE/mean from independent experiments in $n = 3$ HEK cells and $n = 6$ *Xenopus* oocytes. Ratios α_0/α_∞ and β_0/β_∞ are the means of ratios from n cells, not ratios between two means.

TABLE 2 ChR2 conductance ratios α, β, and δ_D in HEK cells

α_0	$2.3 \times 10^6 \pm 16\%$
α_∞	$3.8 \times 10^6 \pm 9\%$
α_0/α_∞	$0.63 \pm 8\%$
β_0	$12 \times 10^{-3} \pm 20\%$
β_∞	$5 \times 10^{-3} \pm 16\%$
β_0/β_∞	$2.3 \pm 8\%$
δ_{D0}/mM	$4.7 \pm 16\%$
$\delta_{D\infty}$/mM	$7.3 \pm 9\%$
$\delta_{D0}/\delta_{D\infty}$	$0.64 \pm 8\%$

$\alpha = k^0_{cH}/k^0_{cM}$ for H^+ over M^+; $\beta = k^0_{cD}/k^0_{cM}$ for D^{2+} ($Ca^{2+} + Mg^{2+}$) over M^+; and δ_D = correction for $[D^{2+}]_e$ determined in HEK cells, from experiments with different concentrations of external Ca^{2+}. Eq. 10 was fit to reversal voltages, E_r, at $[D^{2+}]_e = \delta_D + 0.2$, 2.0, and 20 mM $[Ca^{2+}]_o$, at pH_e 9.0, and to data from experiment in Fig. 5 *B*. Cytoplasmic cation concentrations were 120 mM M^+ (100 K^+ + 20 Na^+) and 2 mM D^{2+} (2 mM Mg^{2+} + 0.25 μM Ca^{2+}), pH_c 7.3. Subscripts 0 and ∞ indicate values from initial and stationary currents, respectively. Values are expressed as means ± percent error, 100·SE/mean from independent experiments in three HEK cells.

of the depolarizing effect of $[Ca^{2+}]_e$ on E_r (Fig. 5 *B*). The numerical analysis of these E_r data was not as straightforward as that from Fig. 4, because the uncertain relations between Mg^{2+} and Ca^{2+} were changing, and the condition $[D^{2+}]_e = 0$ could not be carried out for stability reasons. Nevertheless, after adjustment of $k^0_{cD}[D^{2+}]$ for selectivity variations between Ca^{2+} and Mg^{2+} by introducing δ_D, as described in the legend to Fig. 5 *B*, good fits of Eq. 10 to the experimental data in Fig. 5 *B* were achieved, whereby the amounts and temporal changes of the resulting conductance ratios α and β (Table 2) agree reasonably well with those in Table 1 taken from the experimental results in Fig. 4.

The numerical results of the selectivity relations of ChR2 are compiled in Table 1, for expression in both *Xenopus* oocytes and HEK cells. These results can be summarized as follows:

1. The selectivity relations of ChR2 are similar in both expression systems. This result confirms the notion (7) that i), the protein expresses its typical features, independent of the particular expression system, and ii), the lack of the knowledge of the exact ionic composition in *Xenopus* oocytes does not severely affect the validity of our analysis.
2. Upon a bright light pulse, the initial selectivity α for H^+ over M^+ is ~3×10^6 and increases by a factor of ~2 to its stationary value.
3. Correspondingly, the initial selectivity β for D^{2+} (Mg^{2+} and/or Ca^{2+}) over M^+ is ~0.01 and decreases by a factor of ~2 to its stationary value.
4. With respect to H^+, the decrease of β means another increase of the H^+ selectivity. A temporal increase of the H^+ selectivity during illumination is the global experimental result of this study.

It is expected that changes of the ionic composition of the cytoplasmic medium will reveal consistent conductance ratios. For technical reasons, this could only be examined in HEK cells, for instance, by reducing the internal Na^+ concentration from 120 to 5 mM. The theory for our scenario predicts that this ionic change would shift E_r by about +10 mV toward E_H at pH_e 6.0, i.e., closer to the dashed reference line in the positive branches of Fig. 4 *A*. Corresponding measurements at pH_e 6.0 with and without external Na^+ ($n = 4$ independent samples; data not shown explicitly) confirmed this expectation quantitatively and yielded $\alpha \approx 3 \times 10^6$ and $\beta \approx 10^{-2}$ by fitting Eq. 10 to them, which agrees well with the conductance ratios listed in Tables 1 and 2.

The observed selectivity increase within the photocycle of ChR2 is paralleled by a known decrease of the total conductance (see slopes in Figs. 1 *D*, 2, and 3). This combination suggests that the physiological benefit of this sensory device is that it functions quickly, by employing a rather nonselective conductance at the expense of accuracy initially, and hence more precisely in the case of sufficient stimulus quantity.

The photophobic response of the alga is triggered by sudden light intensity changes and a large transient photoreceptor current that is carried by several ionic species mainly conducted by the open state O_1 (19–21). The same O_1 state should carry in the alga the photoreceptor current responsible for phototaxis at low light, where most of the ChR is in the C_1 state. In contrast, in continuous light of high intensity, the photocurrent is reduced by two regulatory factors: first, by accumulation of late nonconducting photocycle intermediates (3,11,12), and second, by a reduced M^+ and D^{2+} conductance of the O_2 state. Thus, the cell saves energy at high light intensity by restricting the inward photoreceptor current (21,22).

We thank Maila Reh for technical support and preparation of the *Xenopus* oocytes. We thank Dale Sanders for critical reading of the manuscript. We are also indebted to E. Bamberg for sharing the ChR2-HEK cell line with us.

A.B. is supported by a Leibniz Graduate School fellowship. This work was supported by a Deutsche Forschungsgemeinschaft grant (to P.H.).

REFERENCES

1. Hegemann, P. 2008. Algal sensory photoreceptors. *Annu. Rev. Plant Biol.* 59:167–189.
2. Zhang, F., A. M. Aravanis, …, K. Deisseroth. 2007. Circuit-breakers: optical technologies for probing neural signals and systems. *Nat. Rev. Neurosci.* 8:577–581.
3. Ernst, O. P., P. A. Sánchez Murcia, …, P. Hegemann. 2008. Photoactivation of channelrhodopsin. *J. Biol. Chem.* 283:1637–1643.
4. Zhang, F., M. Prigge, …, K. Deisseroth. 2008. Red-shifted optogenetic excitation: a tool for fast neural control derived from *Volvox carteri*. *Nat. Neurosci.* 11:631–633.
5. Tsunoda, S. P., and P. Hegemann. 2009. Glu 87 of channelrhodopsin-1 causes pH-dependent color tuning and fast photocurrent inactivation. *Photochem. Photobiol.* 85:564–569.
6. Lin, J. Y., M. Z. Lin, …, R. Y. Tsien. 2009. Characterization of engineered channelrhodopsin variants with improved properties and kinetics. *Biophys. J.* 96:1803–1814.

7. Nagel, G., T. Szellas, …, E. Bamberg. 2003. Channelrhodopsin-2, a directly light-gated cation-selective membrane channel. *Proc. Natl. Acad. Sci. USA.* 100:13940–13945.

8. Ishizuka, T., M. Kakuda, …, H. Yawo. 2006. Kinetic evaluation of photosensitivity in genetically engineered neurons expressing green algae light-gated channels. *Neurosci. Res.* 54:85–94.

9. Hegemann, P., S. Ehlenbeck, and D. Gradmann. 2005. Multiple photocycles of channelrhodopsin. *Biophys. J.* 89:3911–3918.

10. Nikolic, K., N. Grossman, …, P. Degenaar. 2009. Photocycles of channelrhodopsin-2. *Photochem. Photobiol.* 85:400–411.

11. Bamann, C., T. Kirsch, …, E. Bamberg. 2008. Spectral characteristics of the photocycle of channelrhodopsin-2 and its implication for channel function. *J. Mol. Biol.* 375:686–694.

12. Ritter, E., K. Stehfest, …, F. J. Bartl. 2008. Monitoring light-induced structural changes of channelrhodopsin-2 by UV-visible and Fourier transform infrared spectroscopy. *J. Biol. Chem.* 283:35033–35041.

13. Zheng, J., and F. J. Sigworth. 1997. Selectivity changes during activation of mutant *Shaker* potassium channels. *J. Gen. Physiol.* 110:101–117.

14. Chang, D. C. 1983. Dependence of cellular potential on ionic concentrations. Data supporting a modification of the constant field equation. *Biophys. J.* 43:149–156.

15. Andersen, O. S. 1989. Kinetics of ion movement mediated by carriers and channels. *Methods Enzymol.* 171:62–112.

16. Gradmann, D., H. G. Klieber, and U. P. Hansen. 1987. Reaction kinetic parameters for ion transport from steady-state current-voltage curves. *Biophys. J.* 51:569–585.

17. King, E. L., and C. Altman. 1956. A schematic method of deriving the rate laws for enzyme-catalyzed reactions. *J. Phys. Chem.* 60:1375–1378.

18. Barish, M. E. 1983. A transient calcium-dependent chloride current in the immature *Xenopus* oocyte. *J. Physiol. Lond.* 342:309–325.

19. Nonnengässer, C., E. M. Holland, …, P. Hegemann. 1996. The nature of rhodopsin-triggered photocurrents in *Chlamydomonas*. II. Influence of monovalent ions. *Biophys. J.* 70:932–938.

20. Holland, E. M., H. Harz, …, P. Hegemann. 1997. Control of phobic behavioral responses by rhodopsin-induced photocurrents in *Chlamydomonas*. *Biophys. J.* 73:1395–1401.

21. Sineshchekov, O. A., and E. G. Govorunova. 1999. Rhodopsin-mediated photosensing in green flagellated algae. *Trends Plant Sci.* 4:58–63.

22. Harz, H., and P. Hegemann. 1991. Rhodopsin-regulated calcium currents in *Chlamydomonas*. *Nature.* 351:489–491.